CHEMISTRY OF MATERIALS
Article

Chem. Mater. **2009,** *21,* 4135–4145 4135
DOI:10.1021/cm9012816

Incorporation of Phosphorus into Mesostructured Silicas: A Novel Approach to Reduce the SiO_2 Leaching in Water

Ana García, Montserrat Colilla, Isabel Izquierdo-Barba, and María Vallet-Regí*

Departamento de Química Inorgánica y Bioinorgánica, Facultad de Farmacia, Universidad Complutense de Madrid, E-28040-Madrid, Spain, and Centro de Investigación Biomédica en Red. Bioingeniería, Biomateriales y Nanomedicina, CIBER-BBN, Spain

Received December 19, 2008. Revised Manuscript Received July 24, 2009

Nanostructured mesoporous silica networks with phosphorus substitutions have been obtained through evaporation induced self-assembly (EISA) method using a nonionic surfactant as structure directing agent and triethylorthosilicate and phosphoric acid as SiO_2 and P_2O_5 sources, respectively. Diverse mesopore arrangement symmetries and textural properties have been obtained by modifying the Si/P molar ratio. Therefore mesoporous matrices exhibited an evolution from 3D cubic to 2D hexagonal and wormlike structure with the increase in the substitution degree of the silica network by P_2O_5 centers. Studies carried out by soaking these materials into water at 37 °C revealed that P-containing nanostructured materials, with P_2O_5 contents above 1.25% mol, release smaller amounts of silica to the aqueous medium than pure silica matrix. The increase in the cross-linking degree of the silica network together with the increase of the acid character due to the presence of phosphorus centers could explain the decrease of silica leaching in water. Preliminary in vitro biocompatibility assays in osteoblastic cell culture evidence the lowest cellular damage induced by the sample with the highest P-content. These materials are promising candidates to be applied in diverse technological fields including biomaterials science.

Introduction

Highly ordered mesoporous materials are receiving growing interest by the scientific community since the discovery of M41S family of mesoporous silicas in 1992 by Mobil Oil and Waseda University researchers.[1,2] These materials exhibit outstanding structural and textural properties such as ordered pore networks with narrow pore size distributions, high surface areas, and great pore volumes. These features have made mesoporous materials excellent candidates for a wide range of applications including catalysis, chromatography, lasers, sensors, solar cells, gas storage, adsorption/separation, etc.[3−6] In the past few years, the potential applications of mesoporous materials have been expanded into the biomaterials field for drug delivery[7−10]and bone tissue regeneration technologies.[11,12]

Recent advances in supramolecular chemistry have allowed the increase in the number of available mesostructures with different compositions, large variety of pore arrangements, and symmetries that allow a large versatility of functions and novel features.[3] The structural and textural properties of mesoporous materials are known to depend on a wide number of parameters such as the synthesis method and the chemical nature of the surfactant used as structure-directing agent. Large-pore, three-dimensional (3D) mesoporous silicas synthesized by using amphiphilic block copolymers have recently attracted much attention for potential applications requiring easily accessible, uniform large pore and the possibility to load large molecules such as certain enzymes and proteins.[13,14] Examples of these mesoporous materials are SBA-15, with 2D hexagonal structure (*p6mm* plain group) and interconnected complementary microporosity[15,16] and FDU-5[17,18] with 3D bicontinuous cubic

*Corresponding author. Tel: +34-913941843. Fax: +34-913941786. E-mail: vallet@farm.ucm.es.

(1) Kresge, C. T.; Leonovicz, M. E.; Roth, W. J.; Vartuli, J. C.; Beck, J. S. *Nature* **1992**, *359*, 710–712.
(2) Yanagisawa, T.; Shimizu, T.; Kuroda, K.; Kato, C. *Bull. Chem. Soc. Jpn.* **1990**, *63*, 988–992.
(3) Ying, J. Y.; Mehnert, C. P.; Wong, M. S. *Angew. Chem., Int. Ed.* **1999**, *38*, 56–77.
(4) Davis, M. E. *Nature* **2002**, *417*, 813–821.
(5) Stein, A. *Adv. Mater.* **2003**, *15*, 763–775.
(6) Li, L. L.; Sun, H.; Fang, C. J.; Xu, J.; Jin, J. Y.; Yan, C. H. *J. Mater. Chem.* **2007**, *17*, 4492–4498.
(7) Vallet-Regí, M.; Rámila, A.; del Real, R. P.; Pérez-Pariente, J. *Chem. Mater.* **2001**, *13*, 308–311.
(8) Lai, C. Y.; Trewyn, B. G.; Jeftinija, D. M.; Jeftinija, K.; Xu, S.; Jeftinija, S.; Lin, V. S. Y. *J. Am. Chem. Soc.* **2003**, *125*, 4451–4459.
(9) Vallet-Regí, M.; Balas, F.; Arcos, D. *Angew. Chem., Int. Ed.* **2007**, *46*, 7548–7558.
(10) Vallet-Regí, M. *Chem.—Eur. J.* **2006**, *12*, 5934–5943.
(11) Vallet-Regí, M.; Ruiz-González, L.; Izquierdo-Barba, I.; González-Calbet, J. M. *J. Mater. Chem.* **2006**, *16*, 26–31.
(12) Vallet-Regí, M.; Colilla, M.; Izquierdo-Barba, I. *J. Biomed. Nanotechnol.* **2008**, *4*, 1–15.
(13) Yiu, H. H. P.; Wright, P. A. *J. Mater. Chem.* **2005**, *15*, 3690–3700.
(14) Vallet-Regí, M.; Balas, F.; Colilla, M.; Manzano, M. *Prog. Solid State Chem.* **2008**, *36*, 163–191.
(15) Zhao, D.; Feng, F.; Huo, Q.; Melosh, N.; Fredrickson, G. H.; Chmelka, B. F.; Stucky, G. D. *Science* **1998**, *279*, 548–552.
(16) Liu, Z.; Terasaki, O.; Ohsuna, T.; Hiraga, K.; Shin, H. J.; Ryoo, R. *Chem. Phys. Chem.* **2001**, *2*, 229–231.
(17) Liu, X.; Tian, B.; Yu, C.; Gao, F.; Xie, S.; Tu, B.; Che, R.; Peng, L.-M.; Zhao, D. *Angew. Chem., Int Ed.* **2002**, *18*, 3876–3878.
(18) Sakamoto, Y.; Kim, T. W.; Ryoo, R.; Terasaki, O. *Angew. Chem., Int. Ed.* **2004**, *43*, 5231–5234.

Published on Web 08/18/2009

structure ($Ia\bar{3}d$ space group) composed of an enantiometric pair of 3D mesoporous networks that are interwoven as observed in MCM-48.[19]

Currently, much research effort has been dedicated to the incorporation of different heteroelements into the silica framework to modify the properties of mesoporous matrices.[20,21] Mesoporous silicas modified with tetravalent M(IV) (M = Ti, V, Sn, and Zr) or trivalent M(III) (Al, B, Ga, or Fe) dopants have shown enhanced behavior with interesting applications in catalysis.[20,22,23]Moreover, the incorporation of phosphorus into the silica network has been also proposed as a good strategy to increase the number of acid centers into the mesostructure[24,25] and modify the final properties and catalytic applications of the resulting mesoporous materials.[26−28] Recently, the use of mesoporous silicas containing different heteroatoms has been extended to the biomaterials field. Therefore, the inclusion of 1% of phosphorus into MCM-41 mesoporous silica has been demonstrated to accelerate bioactive response of such material.[29] In addition, multicomponent mesoporous materials in the system $SiO_2-CaO-P_2O_5$, the so-called mesoporous bioactive glasses, have been recently revealed as promising bioceramics for bone tissue engineering technologies.[30−32]

One of the main challenges in the performance of mesoporous materials for certain catalytic and biological applications is the enhancement of their chemical and structural stability in water. Much attention has been dedicated to understand the stability in water of certain silica-based mesoporous materials.[33−35] The high surface areas and low mass content of mesoporous matrices make them especially susceptible to undergo chemical, textural, and structural modifications by interaction with water.

Table 1. Amounts of Reactants Used for the Synthesis of Si_xP_y Material[a]

sample	TEOS (g)	H_3PO_4 (g)
Si_{100}	8.30	
$Si_{98.75}P_{1.25}$	8.17	0.11
$Si_{97.5}P_{2.5}$	7.96	0.23
$Si_{95}P_5$	7.53	0.46

[a] All the syntheses were carried out with 4 g of P123, 1 g of HCl 0.5 N, and 60 g of absolute ethanol.

Recently, the group of Prof. Sanchez has reported the enhanced stability of mixed silica-zirconia and silica−alumina oxide mesoporous materials under biologically relevant conditions compared to pure silica mesoporous matrices.[36] This work evidenced that mixed mesoporous metal oxide films underwent a rapid partial degradation followed by a stabilization of the structure. This final stable interface is especially important when mesoporous materials are intended for bone regeneration applications, where new bone formation and release of biologically agents is targeted. It worth mentioning that the degradation in water of ordered mesoporous materials is tightly related to the amount of silica released to water.

In this work, we have synthesized ordered mesoporous materials in the binary system $SiO_2-P_2O_5$ with different P/Si molar ratios and carried out degradability tests in water. For that reason, the measurement of the quality of silicic acid species in solution versus soaking time in water was performed. The results evidence that the amount of phosphorus incorporated into the silica network governs the structural and textural properties of the resulting mesoporous matrix. This article also reveals that the presence of PO_4 units in the mesoporous materials results in materials with reduced silica leaching in water compared to pure silica matrices. These findings make these novel mesoporous matrices excellent candidates to be applied in catalysis and biomaterials fields.

Materials and Methods

Synthesis. Ordered mesoporous materials in the binary system $SiO_2-P_2O_5$ were synthesized by using a nonionic surfactant Pluronic P123 (BASF) as structure-directing agent and evaporation induced self-assembly (EISA) method.[37] P123 is an amphiphilic triblock polymer exhibiting the sequence $EO_{20}PO_{70}EO_{20}$, where EO is poly(ethylene oxide) and PO is poly(propylene oxide). Tetraethyl orthosilicate (TEOS, Aldrich) and phosphoric acid (H_3PO_4, Fluka) were used as SiO_2 and P_2O_5 sources, respectively. In a typical synthesis 4 g of P123 were dissolved in 60 g of ethanol containing 1 g of HCl 0.5 M and the corresponding amount of H_3PO_4. Subsequently, the appropriate amount of TEOS was added under continuous stirring. The different amounts of reactive employed for the syntheses are shown in Table 1. The TEOS/H_3PO_4 molar ratio was varied to obtain the different materials (whereas the total molar ratio TEOS + H_3PO_4 was kept constant). The resulting colorless sols were stirred at room temperature for 24 h and then transferred into Petri dishes (9 cm diameter) and evaporated at room temperature during 7 days. Finally, transparent membranes of 1 mm of

(19) Kaneda, M.; Tsubakiyama, T.; Carlsson, A.; Sakamoto, Y.; Ohsuna, T.; Terasaki, O. *J. Phys. Chem. B* **2002**, *106*, 1256–1266.
(20) Tuel, A. *Microporous Mesoporous Mater.* **1999**, *27*, 151–169.
(21) Soler-Illia, G. J. A. A.; Sanchez, C.; Lebeau, B.; Patarin, J. *Chem. Rev.* **2002**, *102*, 4093–4138.
(22) Katovic, A.; Giordano, G.; Bonelli, B.; Onida, B.; Garrone, E.; Lentz, P.; Nagy, J. B. *Microporous Mesoporous Mater.* **2001**, *44−45*, 275–281.
(23) Nowak, I.; Ziolek, M.; Jaroniec, M. *J. Phys. Chem. B* **2004**, *108*, 3722–3727.
(24) Corriu, R. J. P.; Hoarau, C.; Mehdi, A.; Reyé, C. *Chem. Commun.* **2000**, 71–72.
(25) Wu, P.; Liu, Y.; He, M.; Iwamoto, M. *Chem. Mater.* **2005**, *17*, 3921–3928.
(26) Pang, J. B.; Qiu, K. Y.; Wei, Y.; Lei, X. J.; Liu, Z. F. *Chem. Commun.* **2000**, 477–478.
(27) Colilla, M.; Balas, F.; Manzano, M.; Vallet-Regí, M. *Chem. Mater.* **2007**, *19*, 3099–3101.
(28) Xiong, L.; Yang, Y.; Shi, J.; Nogami, M. *Microporous Mesoporous Mater.* **2008**, *111*, 343–349.
(29) Vallet-Regí, M.; Izquierdo-Barba, I.; Rámila, A.; Pérez-Pariente, J.; Babonneau, F.; González-Calbet, J. M. *Solid State Sci.* **2005**, *7*, 233–237.
(30) Yan, X.; Yu, C.; Zhou, X.; Tang, J.; Zhao, D. *Angew. Chem., Int. Ed.* **2004**, *43*, 5980–5984.
(31) López-Noriega, A.; Arcos, D.; Izquierdo-Barba, I.; Sakamoto, Y.; Terasaki, O.; Vallet-Regí, M. *Chem. Mater.* **2006**, *18*, 3137–3144.
(32) Izquierdo-Barba, I.; Arcos, D.; Sakamoto, Y.; Terasaki, O.; López-Noriega, A.; Vallet-Regí, M. *Chem. Mater.* **2008**, *20*, 3191–3198.
(33) Cassiers, K.; Linssen, T.; Mathieu, M.; Benjelloun, M.; Schrijnemakers, K.; Van Der Voort, P.; Cool, P.; Vansant, E. F. *Chem. Mater.* **2002**, *14*, 2317–2324.
(34) Zhang, F.; Yan, Y.; Yang, H.; Meng, Y.; Yu, C.; Tu, B.; Zhao, D. *J. Phys. Chem. B* **2005**, *109*, 8723–8732.
(35) Galarneau, A.; Nader, M.; Guenneau, F.; Di Renzo, F.; Gedeon, A. *J. Phys. Chem. C* **2007**, *111*, 8268–8277.
(36) Bass, J. D.; Grosso, D.; Boissiere, C.; Belamie, E.; Coradin, T.; Sanchez, C. *Chem. Mater.* **2007**, *19*, 4349–4356.
(37) Brinker, C. J.; Lu, Y. F.; Sellinger, A.; Fan, H. Y. *Adv. Mater.* **1999**, *11*, 579–585.

thickness were obtained and calcined at 550 °C in air for 6 h to finally obtain the ordered mesoporous powders. Following this method, five different compositions were synthesized, which were denoted as Si_xP_y where x and y are the nominal composition (% in mol) of SiO_2 and P_2O_5, respectively.

Characterization. The resulting samples were characterized by powder X-ray diffraction (XRD) in a Philips X′Pert diffractometer equipped with a Cu Kα radiation (wavelength 1.5406 Å). XRD patterns were collected in the 2θ range between 0.6° and 10° with a step size of 0.02° and counting time of 5 s per step. Transmission electron microscopy (TEM) was carried out with a JEOL 3000 FEG electron microscope fitted with a double tilting goniometer stage (±45°) and with an Oxford LINK EDS analyzer. TEM images were recorded using a CCD camera (MultiScan model 794, Gatan, 1024 × 1024 pixels, size 24 μm × 24 μm) using low-dose condition. Fourier Transform (FT) patterns were conducted using the Digital Micrograph (Gatan) software. The textural properties of the calcined materials were determined by N_2 adsorption/desorption analyses at −196 °C on a Micromeritics ASAP 2020 instrument (Micromeritics Co, Norcross, USA). In all cases, 50−100 mg of materials were degassed during 24 h at 200 °C under a vacuum lower than 0.3 kPa before the analysis. The total pore volume of samples was estimated from the amount of N_2 adsorbed at a relative pressure of 0.97. The surface area was determined using the Brunauer−Emmett−Teller (BET) method. The average mesopore size (D_P) was obtained from the maximum of the pore size distribution (PSD) calculated from the adsorption branch of the isotherm by means of the Barrett−Joyner−Halenda (BJH) method.[38] To assess the possible existence of micropores (pore diameter <2 nm) in our samples, we carried out the t-plot method.

The total phosphorus and silicon contents in the calcined powders were determined by X-ray fluorescence (XRF) using a Philips PANalytical AXIOS spectrometer (Philips Electronics NV). X-rays were generated using the RhKα line at $\lambda = 0.614$ Å. Energy-disperse X-ray spectroscopy (EDS) was also used to semiquantitatively determine the chemical composition of the materials and was performed by using an Oxford model ISIS coupled to the JEOL 3000 FEG electron microscope. Fourier transform infrared (FTIR) spectroscopy was carried out to determine the chemical nature of phosphorus species in the samples. FTIR spectra were collected in a Thermo Nicolet Nexus equipped with a Goldengate attenuated total reflectance (ATR) device. ^{29}Si and ^{31}P single pulse (SP)/MAS (magic angle spinning) solid-state nuclear magnetic resonance (NMR) measurements were performed to evaluate the different silicon and phosphorus environments in the synthesized samples. The NMR spectra were recorded on a Bruker Avance 400 spectrometer. Samples were spun at 10 kHz for ^{29}Si and 6 kHz in the case of ^{31}P. Spectrometer frequencies were set to 79.49 and 161.97 MHz for ^{29}Si and ^{31}P, respectively. Chemical shift values were referenced to tetramethylsilane (TMS) and H_3PO_4 for ^{29}Si and ^{31}P, respectively. The time period between successive accumulations was 5 and 4 s for ^{29}Si and ^{31}P, respectively, and the number of scans was 10000 for all spectra. Thermogravimetric analyses (TG) were carried out in a dynamic air atmosphere between 30 and 1000 °C (flow rate of 100 mL/min with a heating rate of 10 °C/min) using a Perkin-Elmer Diamond analyzer.

The zeta-potential (ζ) measurements were performed in a Zetasizer Nano Series instrument coupled to a MPT-2 multipurpose titrator from Malvern. ζ-potential can be described by Smoluchowski's equation:[39] $\zeta = 4\pi\eta U/\varepsilon$, where U is the electrophoretic mobility, η is the viscosity of water, and ε is the dielectric constant of water. Five milligrams of each Si_xP_y mesoporous powders was added to 10 mL of KCl 10 mM (used as the supporting electrolyte); the pH was adjusted by adding appropriate volumes of 0.10 M HCl or 0.10 M KOH solutions.

Degradability Test Studies in Water at 37 °C. Before performing the degradability tests in water at 37 °C, all materials were gently washed during 3 h in Milli-Q water under continuous orbital stirring to avoid the initial burst release effect of different highly soluble phosphorus and/or silicon species that would leach out from materials to water. During the washing process, the pH variations of water were monitored. The results showed that there was an immediate release of soluble species, which led to a pH decrease during the first few minutes of assay. After that, the pH remained constant for the rest of the washing period (see graph inset Figure 7). Therefore, this kind of initial washing-in-water pretreatment is sometimes necessary to avoid the release of high concentrations of ions in solutions, for instance when these matrices are employed as biomaterials in cell culture assays.[40] The amount of phosphorus remaining in samples after the washing process was determined by XRF. Subsequently, the influence of phosphorus incorporation in the degradability of mesoporous silica materials in water was evaluated by soaking 500 mg of powders into 200 mL of Milli-Q water (Millipore) at 37 °C under continuous orbital stirring in an Ecotron HT incubator. After 72 h of incubation, the powdered samples were recovered and left to dry at room temperature. Moreover, the variation of the pH in water was measured in an Ilyte Na^+, K^+, Ca^{2+}, pH analyzer and the variations in the powdered samples were characterized by XRD, N_2 adsorption, NMR, and XFR after water treatment. The SiO_2 concentration leached to water versus time was monitored by colorimetric analysis based on US EPA 370.1 method in the 0.1−10 mg/L range at a wavelength of 660 nm. The orthophosphate concentration released to water versus time was also colorimetrically determined by the US EPA 365.3 method in the 0.01−0.50 mg/L range at a wavelength of 880 nm. For these measurements a SmartChem140 automatic discrete analyzer (Alliance Instruments, AMS France) was employed. All the studies were carried out in water under mild conditions (37 °C) by soaking 50 mg of each powdered material into 100 mL of water. To minimize the influence of the pH variations in the SiO_2 release behavior from different Si_xP_y samples the pH of water was externally acidified up to pH 3.5 using H_3PO_4 for the delivery assays of Si_{100} sample. Moreover, to reduce the effect of pH in the SiO_2 release from $Si_{98.75}P_{1.25}$ and $Si_{97.5}P_{2.5}$ materials the pH of water was also adjusted to 3.5 in both cases, which is the pH that water reaches after immersion of $Si_{95}P_5$ sample (see Figure 7). Three independent experiments were carried out for each Si_xP_y material and duplicated measurements at different times of all samples were performed. The average value of six SiO_2 concentration measurements at each time with the corresponding error bar at each time for each Si_xP_y sample was then calculated.

In vitro Biocompatibility Assays. We cultured human osteoblast-like cell line (HOS) from European Collection of Cell Cultures (ECACC, no. 87070202), in presence of different Si_xP_y

(38) Barrett, E. P.; Joyner, L. G.; Halenda, P. H. *J. Am. Chem. Soc.* **1951**, *73*, 373–381.

(39) Smoluchowski, M. V. Elektrische Endosmose und Stromungsstrome. In *Handbuch der Electrizitat und des Magnetismus*; Barth: Leipzig, Germany, 1921.

(40) Olmo, N; Martín, A. I.; Salinas, A. J.; Turnay, J.; Vallet-Regí, M.; Lizarbe, M. A. *Biomaterials* **2003**, *24*, 3383–3393.

powdered materials. Lactate deshidrogenase activity (LDH) and 3-[4,5-dimethyl-thiazol-2-yl]-2,5-diphenyltetrazolium bromide (MTT) assays were performed to study the biocompatibility of such materials.[41,42] With the aim to determine the influence of the chemical nature of the different mesoporous surfaces on the cellular response, and therefore discriminate the effect of the particle size, a homogeneous fraction with particle size between 80 and 40 μm was used in these in vitro tests. According to the silica leaching results carried out in water, which evidenced that Si_{100} and $Si_{98.75}P_{1.25}$ samples exhibited analogous silica release behaviors, the samples selected to perform the in vitro biocompatibity tests were Si_{100}, $Si_{97.5}P_{2.5}$, and $Si_{95}P_5$.

Previously to biocompatibility assays, the powdered samples were sterilized by heating at 180 °C for 24 h and then washed during 3 h in Dulbecco's modified Eagle medium (DMEM) to eliminate the unspecific bonding phosphorus and silica species as was previously commented.

Briefly, the HOS cells were first seeded in 24-well with DMEM containing 2 mM glutamine, 100 U/mL penicillin, 100 g/mL streptomycin, and 10% fetal calf serum (FCS) at 37 °C in a humidified atmosphere of 95% air and 5% CO_2. The initial density was 5×10^3 cells/plate. After 24 h in culture, Si_{100}, $Si_{97.5}P_{2.5}$, and $Si_{95}P_5$ materials were added at different concentrations (1.25, 2.5, 6.25, and 12.5 mg/mL). Different cellular aspect were analyzed to know the cell viability during cell cultures in presence of each Si_xP_y material. Cytotoxicity tests, by determination of lactate dehidrogenase (LDH) activity in the culture medium after 2 days of assays, were performed using a commercially available kit (Spinreact), and cell proliferation determination was carried out by using the MTT assays after 2 and 6 days of incubation in culture medium. Both measurements, LDH activity and mitochondrial function by reduction of MTT reagent, were assessed using an UNICAM UV-500 UV−visible spectrophotometer by measuring the absorbance at 340 and 570 nm, respectively. Moreover, silicon release in culture medium was colorimetrically determined by using a Smart-Chem140 analyzer using the EPA method above-mentioned.

Results and Discussion

Characterization. The structural characterization of the synthesized Si_xP_y samples reveals that different mesoporous arrangements can be obtained as a function of the phosphorus content. For simplicity, each structure is discussed in turn in the text as follows. The XRD pattern of pure silica Si_{100} sample (Figure 1a) shows three diffraction maxima at 2θ values of 0.86, 1.11, and 2.04°, which can be indexed as 200, 211, and 400 reflections of a cubic structure, respectively. The unit-cell parameter (a_0) calculated from 211 peak positions is 19.6 nm. $Si_{98.75}P_{1.25}$ sample exhibits a XRD profile comparable to that of Si_{100} sample and an a_0 value of 17.2 nm. Figure 2a−d shows TEM images and their corresponding FT difractograms with the incident electron beam parallel to the [111] and [531] directions for the Si_{100} sample, and to the [100] and [531] directions for the $Si_{98.75}P_{1.25}$ sample. TEM images and FT diagrams could correspond to a 3D bicontinuous cubic $Ia\bar{3}d$ symmetry similar to that of MCM-48[19] and

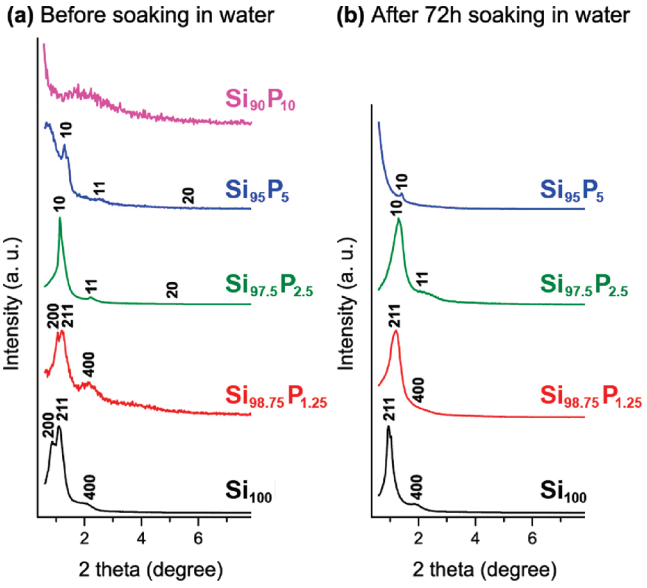

Figure 1. Powder XRD diffraction patterns for Si_{100} and Si_xP_y materials before and after 72 h soaked in water.

FDU-5[18] mesoporous materials. However, some very slights deviations from this symmetry are observed in the FT diagrams. In both cases the 200 and 110 reflections, which are extinguished in a conventional $Ia\bar{3}d$ symmetry, can be observed in the different FT diagrams. Therefore, the FT diagrams clearly show the condition for observable reflections: hkl, $h + k + l = 2n$; $0kl$, $k + l = 2n$; hhl, $l = 2n$; $h00$, $h = 4n$. From these observations, the space-group symmetries were determined to be $I2_13$, according to the International Table for Crystallography which is $Ia\bar{3}d$ subfamily.[43] In this case, follows a 3D cubic bicontinuous network with *G*-surface similar to $Ia\bar{3}d$ symmetry but with a very small deviation from this structure, therefore that we can assume $Ia\bar{3}d$ structure as previously reported.[32] XRD pattern of $Si_{97.5}P_{2.5}$ sample is a typical 2D hexagonal *p6mm* mesophase (Figure 1a) in which the well-resolved peaks at $1:3^{1/2}:2$ *d*-spacing ratios can be indexed as 10, 11, and 20 reflections of a hexagonal structure with a unit-cell parameter of 8.97 nm. TEM images of this sample obtained with the electron beam parallel and perpendicular to the mesoporous channels axis show well ordered hexagonally arranged mesostructures (images e and f in Figure 2). XRD pattern of $Si_{95}P_5$ sample shows two low-intensity diffraction peaks which could be indexed by assuming 2D hexagonal arrangement and TEM studies confirm the coexistence of two different phases. The main phase would correspond to a 2D hexagonal symmetry (*p6mm*) with a unit-cell parameter of 7.87 nm. The second phase would correspond to poorly order wormlike aggregates (images g and h in Figure 2). Finally, XRD pattern of the sample synthesized with the highest H_3PO_4 amounts ($Si_{90}P_{10}$ sample) does not show any diffraction peak, which is typical of an amorphous material with a lack of mesostructural arrangement as confirmed by TEM showing a wormlike phase in this sample (data not shown).

(41) Arcos, D; Sánchez-Salcedo, S.; Izquierdo-Barba, I.; Ruiz, L.; González-Calbet, J. M.; Vallet-Regí, M. *J. Biomed. Mater. Res., Part A* **2006**, *78*, 762–771.
(42) Izquierdo-Barba; Conde, F.; Olmo, N.; Lizarbe, M. A.; García, M. A.; Vallet-Regí, M. *Acta Biomater.* **2006**, *2*, 445–455.
(43) *International Tables for Crystallography, Volume A Space Group Symmetry*; Hahn, T., Ed.; Kluwer Academic: Dordrecht, The Netherlands, 1992.

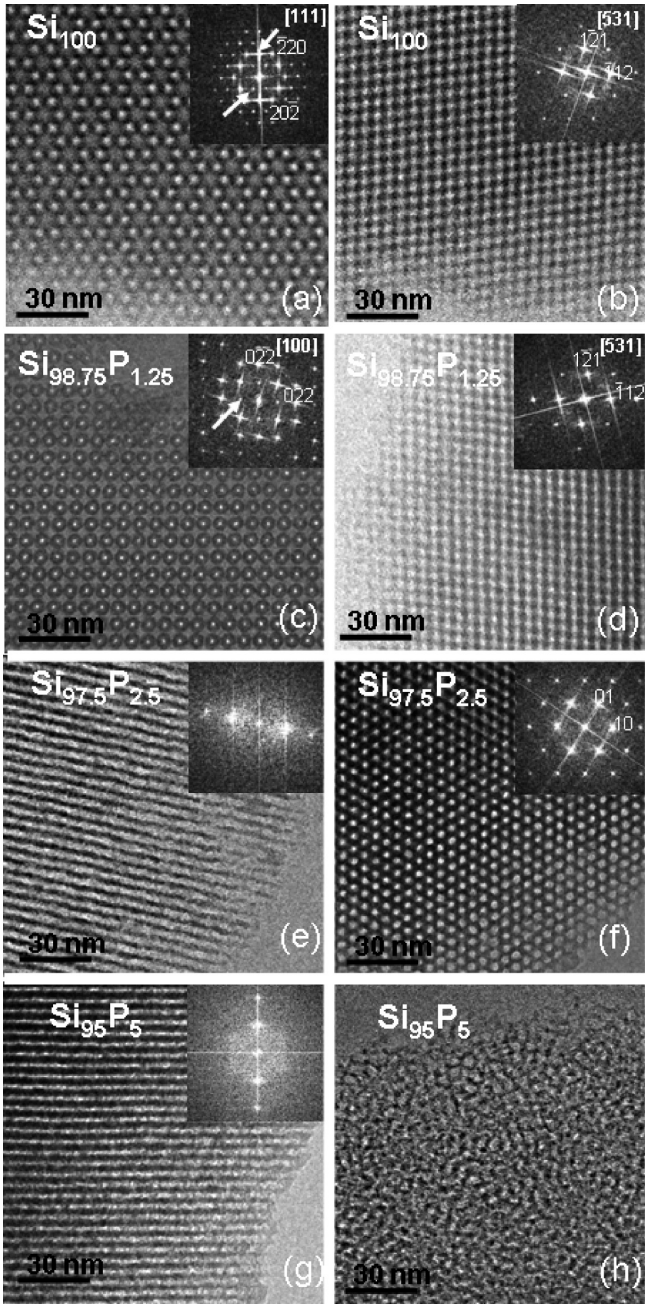

Figure 2. TEM images of Si_xP_y materials and their corresponding FT difractograms. The arrows show the 110 and 200 reflections.

These findings resulting from XRD and TEM evidence that the structural features of Si_xP_y mesoporous materials depend on the phosphorus content, i.e., a progressive evolution from 3D bicontinuous cubic structure, to 2D hexagonal structure and totally lost of mesoporore arrangement is observed. Moreover, there is a remarkable decrease in the a_0 value from 19.6 to 7.87 nm (Table 2), which is caused by the evolution of 3D cubic to 2D hexagonal structure when phosphorus ($y \geq 2.5$) is incorporated into the silica network. Similar results have been previously reported when other heteroatoms are incorporated into the silica network.[44,45]

Textural properties of the Si_xP_y mesoporous materials have been performed by N_2 adsorption. Figure 3 shows the N_2 adsorption isotherms for Si_xP_y samples. All curves can be identified as type IV isotherms according to the IUPAC classification, which are typical for mesoporous solids.[46] The presence of a H1 type hysteresis loops in the mesopore range indicates open-ended cylindrical mesopores characteristics of 3D bicontinuous cubic and 2D hexagonal structures which have been confirmed by XRD and TEM. Table 2 summarizes the symmetry of Si_xP_y samples ($y \leq 5$) and the textural properties obtained from the treatment of N_2 adsorption and XRD data. The analysis of the textural data indicates that the slight variations in the BET surface areas of Si_xP_y materials for $y \leq 2.5$ do not follow any significant trend. These S_{BET} values remain in the 415−390 m^2/g range independently of the P_2O_5 content. However, the S_{BET} value of the sample with the highest P_2O_5 content ($Si_{95}P_5$) experiences a noticeable decrease to 270 m^2/g. Concerning the total pore (V_P) and micropore ($V_{\mu P}$) volumes of Si_xP_y samples, the higher the P_2O_5 content the smaller the pore volumes. The comparison of the pore sizes of Si_{100} and $Si_{98.75}P_{1.25}$ samples, which exhibit 3D bicontinuous cubic structures, evidence that the incorporation of P_2O_5 into the mesoporous silica network leads to a decrease in the D_P from 6.70 to 5.25 nm. However, $Si_{97.5}P_{2.5}$ and $Si_{95}P_5$ samples, with 2D hexagonal structure, exhibit pore diameters of 5.50 and 6.20 nm, respectively. In this case, the increase in the pore size with the phosphorus content can be ascribed to the coexistence of wormlike phases together with 2D hexagonal in $Si_{95}P_5$ sample, as confirmed by TEM studies. The wall thicknesses (t_{wall}) were calculated from the main mesopore sizes and the unit-cell parameters (a_0) derived from XRD measurements, and using the corresponding expressions described in the footnotes of Table 2.[47,48] There are not significant variations in the t_{wall} for 3D bicontinuous cubic structures, with values of around 3 nm for both Si_{100} and $Si_{98.75}P_{1.25}$ samples. The increase in the phosphorus content in $Si_{97.5}P_{2.5}$ sample, with 2D hexagonal symmetry, leads to a slight increase in the t_{wall} to 3.47 nm. Finally, the decrease in the wall thickness to 1.67 nm for $Si_{95}P_5$ sample would agree with the coexistence of 2D hexagonal *p6mm* and wormlike phase in this sample, as evidenced by TEM (images g and h in Figure 2).

In general, the analysis of the textural data of the different Si_xP_y mesoporous matrices are consistent with previous observations in which the effective incorporation of heteroelements to some extent into the mesoporous silica framework generally led to a decrease in the textural properties of the resulting materials.[20,27]

The presence of phosphorus in the mesoporous networks was confirmed by XRF, and EDS analyses and SiO_2 and P_2O_5 % molar values derived from these

(44) Shen, S. C.; Kawi, S. *J. Phys Chem. B* **1999**, *103*, 8870–8876.
(45) Mokaya, R. *J. Phys Chem. B* **2000**, *104*, 8279–8286.
(46) Rouquerol, F.; Rouquerol, J.; Sing, K. *Adsorption by Powders and Porous Solids*; Academic Press: San Diego, 1999.
(47) Ravikovitch, P. I.; Neimark, A. V. *Langmuir* **2000**, *16*, 2419–2423.
(48) Kruk, M.; Jaroniec, M.; Sayari, A. *Chem. Mater.* **1999**, *11*, 492–500.

Table 2. Textural Parameters of Si_{100} and Si_xP_y Samples Obtained from N_2 Adsorption Isotherms before an after Soaking 72 h in Water[a]

material	symmetry	S_{BET} (m^2/g)	V_P (cm^3/g)	$V_{\mu P}$ (cm^3/g)	D_P (nm)	a_0 (nm)	t_{wall} (nm)
b_{100}	$Ia\bar{3}d$	409	0.647	0.0097	6.70	19.6	2.99
Si_{100} (72 h)	$Ia\bar{3}d$	398	0.728	0.0220	6.34	22.8	4.15
Si_bP_b	$Ia\bar{3}d$	415	0.589	0.0070	5.25	17.2	2.94
$Si_{98.75}P_b$ (72 h)	$Ia\bar{3}d$	412	0.565	0.0006	4.80	17.9	3.39
$Si_{97.5}P_{2.5}$	*p6 mm*	390	0.564	0.0015	5.50	8.97	3.47
$Si_{97.5}P_{2.5}$ (72 h)	*p6 mm*	390	0.574	0.0010	5.20	8.48	3.28
$Si_{95}P_5$	*p6 mm* + wormlike	270	0.512	0.0015	6.20*	7.87	1.67
$Si_{95}P_5$ (72 h)	*p6mm*+ wormlike	183	0.509	0.0123	6.80*	8.20	1.40

[a] S_{BET} is the surface area determined by using the BET method. V_P and $V_{\mu P}$ are respectively, the total pore volume and micropore volume obtained using the t-plot method. D_P is the pore diameter calculated by means of the BJH method from the adsorption branch of the isotherm. a_0 is the unit cell parameter calculated by XRD, being $a_0 = \sqrt{6}d_{211}$ and $a_0 = 2/\sqrt{3}d_{10}$ for cubic $Ia\bar{3}d$ and hexagonal *p6mm* structures, respectively. t_{wall} is the wall thickness calculated using the equation $t_{wall} = (a_0/3.0919) - (D_P/2)$ for cubic $Ia\bar{3}d$ structures[47] and the equation $t_{wall} = a_0 - D_P$ for hexagonal *p6mm* structures.[48]

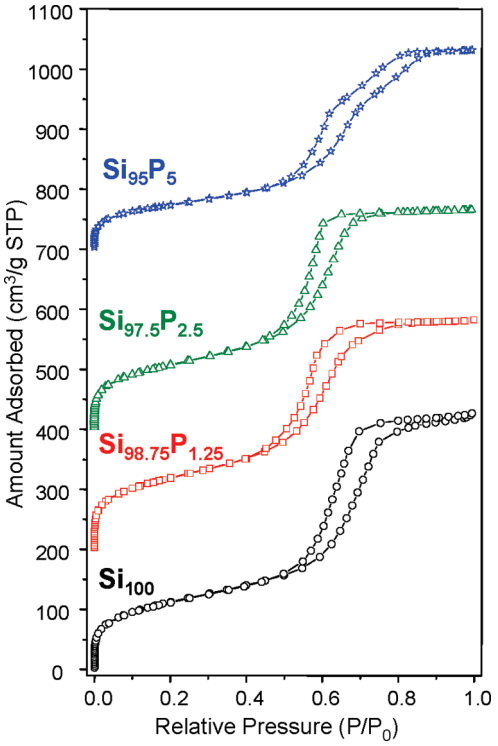

Figure 3. N_2 adsorption isotherms of Si_xP_y materials ($y \leq 5$). The isotherms for samples $Si_{98.75}P_{1.25}$, $Si_{97.5}P_{2.5}$, and $Si_{95}P_5$ were vertically offset by 200, 400, and 700 cm^3/g STP, respectively.

Table 3. Different Molar Percentages of Si_{100} and Si_xP_y Materials Calculated Using XRF and EDS

	nominal (% mol)		XRF (% mol)		EDS (% mol)	
sample	SiO_2	P_2O_5	SiO_2	P_2O_5	SiO_2	P_2O_5
Si_{100}	100		100		100	
$Si_{98.75}P_{1.25}$	98.75	1.25	97.78	2.22[a]	98.65	1.35
$Si_{97.5}P_{2.5}$	97.5	2.5	95.87	4.13[a]	97.10	2.90
$Si_{95}P_5$	95	5	94.30	5.70[a]	94.05	5.95

[a] Note that the phosphorus molar composition is higher than the value obtained by EDS.

measurements, are collected in Table 3. The experimental data are in reasonable agreement with the theoretical compositions. However, in the case of P-containing (Si_xP_y) samples, the percentage of P_2O_5 determined by XRF is higher than that measured by EDS. This fact could be explained by considering the existence of free H_3PO_4 species that would not be incorporated into the

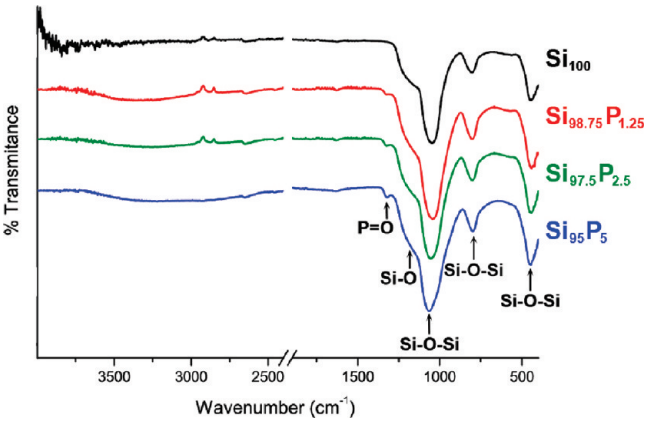

Figure 4. FTIR spectra of Si_xP_y mesoporous materials in a dry atmosphere.

mesostructure. The presence of H_3PO_4 in P-containing samples was confirmed by NMR, as will be commented on below.

To determine the chemical nature of the synthesized materials, we performed a study by FTIR and NMR analyses. FTIR spectra corresponding to calcined Si_xP_y materials are displayed in Figure 4. All samples shows three bands at 1080, 800, and 450 cm^{-1} that can be assigned to the asymmetric Si−O−Si stretch, the symmetric Si−O−Si stretch, and the Si−O−Si deformation mode, respectively. However, in the case of $SiO_2-P_2O_5$ systems, the spectra show a new band at 1330 cm^{-1} that can be ascribed to stretching vibration of P═O groups in a silicophosphate framework.[49] Moreover, the bands at 800 and 445 cm^{-1} could be also attributed to bending modes of P−O−P, Si−O−P, and O−P−O units and to a combination of Si−O−P and Si−O−Si, respectively.[49,50] These results suggest that the structure of $SiO_2-P_2O_5$ systems could consist of a mixed framework, built of [SiO_4] and [PO_4] tetrahedra with one oxygen being linked by a double-bonded phosphorus (P═O).[51]

For further establishing the chemical nature of the silica networks, we recorded ^{29}Si SP/MAS NMR spectra

(49) Chakraborty, I. N.; Condrate, R. A. *Phys. Chem. Glasses* **1985**, *26*, 68–73.
(50) DAppuzzo, M. D.; Aronne, A.; Esposito, S.; Pernice, P. *J. Sol−Gel Sci.* **2000**, *17*, 247–254.
(51) Aronne, A.; Turco, M.; Bagnasco, G.; Pernice, P.; Di Serio, M.; Clayden, N. J.; Marenna, E.; Fanelli, E. *Chem. Mater.* **2005**, *17*, 2081–2090.

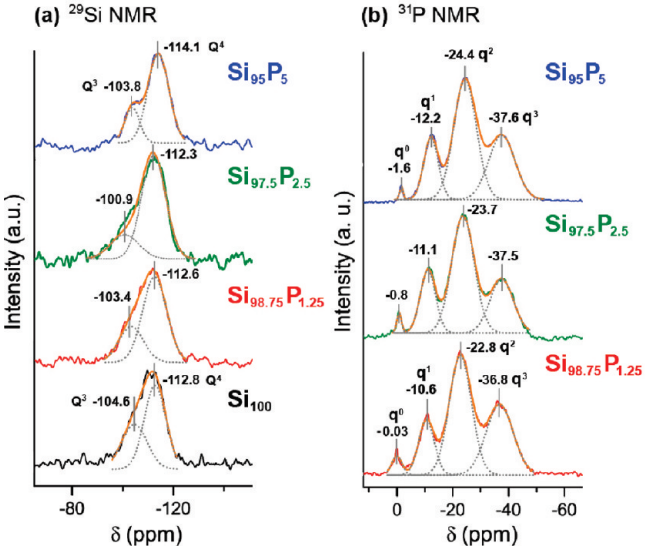

Figure 5. (a) ^{29}Si MAS NMR and (b) ^{31}P MAS NMR spectra of Si_xP_y samples. The component peaks obtained from spectral deconvolutions are displayed by gray dotted lines.

of the different Si_xP_y samples (Figure 5a). ^{29}Si NMR of Si_xP_y materials ($y \leq 2.5$) display signals at ca. −104 ppm and ca. −112 ppm that can be assigned to $Si(OSi)_3(OH)$ (Q^3) or $Si(OSi)(OP)(OH)_2$ and $Si(OSi)_4$ (Q^4) or $Si(OSi)_2(OP)(OH)$ in agreement with recent studies performed by Coelho et al.[52] When the amount of phosphorus increases in the $Si_{95}P_5$ sample, it can be observed that there is a shift in the signal at ca. −112 toward upfields (ca. −114 ppm), which could be related to $Si(OSi)_{4-x}(OP)_x$, with $x = 1-3$, indicating that the P atoms could be cross-linked with the silica network.[26,53]

To determine the state of PO_4 units in the P-containing samples, we recorded ^{31}P SP/MAS NMR spectra. Figure 5b displays ^{31}P NMR spectra of samples, which exhibit three signals at ca. −11 (q^1), −24 (q^2), and −37 ppm (q^3), which are, respectively, due to terminal $O=P(OH)_2(OP \text{ or } OSi)$, $O=P(OH)(OP \text{ or } OSi)_2$, or $O=P(OP)_j(OSi)_k$, with $j + k = 3$.[54] Moreover, a signal at ca. 0 ppm (q^0), which is assigned to H_3PO_4, is observed in the ^{31}P NMR spectra. The presence of H_3PO_4 species would explain the divergence in the phosphorus contents obtained by EDS and XRF. In the case of EDS analyses, the species studied correspond only to ordered mesophase, whereas XRF analyses correspond to the complete sample. These NMR studies suggest that the PO_4 and SiO_4 units would be cross-linked forming covalent networks in P-containing samples, although the direct synthesis of Si−O−P mesoporous materials has been very rarely reported in the literature.[29,52,54]

Degradability Tests in Water at 37 °C. Degradability test in water of Si_xP_y materials were carried out by soaking powder materials into water under orbital stirring at 37 °C,

(52) Coelho, C.; Azais, T.; Bonhomme, C.; Bonhomme-Coury, L.; Boissière, C.; Laurent, G.; Massiot, D. *C. R. Chim.* **2008**, *11*, 387–397.
(53) Szu, S. P.; Klein, L. C.; Greenblatt, M. *J. Non-Cryst. Solids* **1992**, *143*, 21–30.
(54) Neeraj, O.; Eswaramoorthy, M.; Rao, C. N. R. *Mater. Res. Bull.* **1998**, *33*, 1549–1554.

Table 4. XRF Data (mol %) of the Si_xP_y materials before, after Initial Water Washing (3 h), and after 72 h of Water Stability Assay

	before soaking in H_2O		after initial washing		after 72 h of stability assay	
sample	SiO_2	P_2O_5	SiO_2	P_2O_5	SiO_2	P_2O_5
Si_{100}	100		100		100	
$Si_{98.75}P_{1.25}$	97.78	2.22	99.11	0.89	99.20	0.80
$Si_{97.5}P_{2.5}$	95.75	4.25	98.19	1.81	98.37	1.63
$Si_{95}P_5$	94.30	5.70	96.64	3.36	96.76	3.24

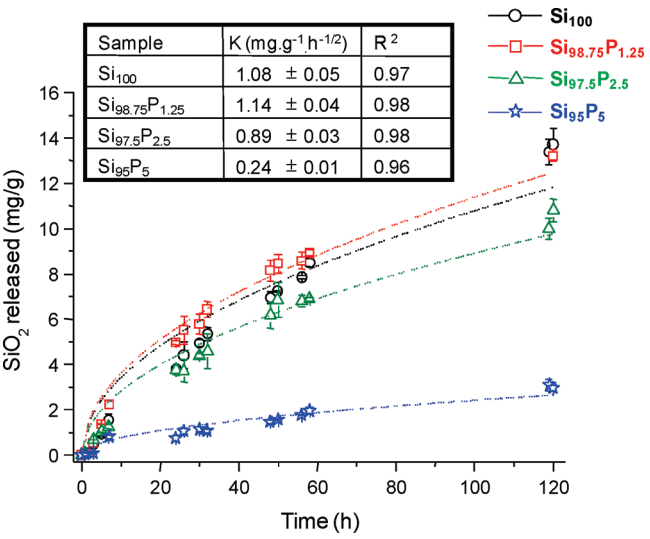

Figure 6. Amount of silica released (mg per gram of mesoporous material) released to water at several times from different Si_xP_y samples. Inset table containing the release kinetic constants (K, $h^{-1/2}$) and the corresponding regression coefficients after fitting the results to the Higuchi diffusion model ($a = Kt^{1/2}$), where a is amount of SiO_2 released after time t and K is the release kinetic constant.[55]

as previously commented. As described in the experimental section, before carrying out the stability tests in water, the powdered samples were submitted to a washing treatment of 3 h in water. The XRF studies (Table 4) reveal that during the washing treatment there is a loss of phosphorus species in the different P-containing samples, which could be ascribed to the removal of the free H_3PO_4 species detected by NMR and also to P_2O_5 species weakly cross-linked that would be easily leached to water. The amounts of phosphorus remaining in $Si_{98.75}P_{1.25}$ and $Si_{97.5}P_{2.5}$ samples after the washing process were ca. 40% in both cases, whereas this amount was ca. 60% for $Si_{95}P_5$ sample. This fact would be in agreement with the higher cross-linking degree observed in the $Si_{95}P_5$ sample by NMR experiments.

The degradability in water of Si_xP_y samples was determined as a function of the amounts of silicon and phosphorus released to the aqueous medium at 37 °C ("mild" conditions) after different incubation times. Moreover, the structural and chemical stabilities of samples were also determined by XRD, N_2 adsorption and NMR studies for final powder after 72 of soaking in water at 37 °C.

Figure 6 shows the amount of SiO_2 released (in milligrams per gram of mesoporous material) as a function of the incubation time in water. The delivery patters reveal

that similar SiO_2 release profiles are observed in pure silica Si_{100} material and the sample with the smallest phosphorus content, $Si_{98.75}P_{1.25}$. Moreover, the release kinetics parameters, derived from the adjust of experimental data to Higuchi equation,[55] are not significantly different in both samples, with the corresponding release kinetic constants (K) being close to 1.1 mg g^{-1} $h^{-1/2}$. When the amount of P_2O_5 phosphorus increases to 2.5 (% mol) in sample $Si_{97.5}P_{2.5}$, the SiO_2 release constant, K, which is tightly related to the release rate, decreases to around 0.9 mg g^{-1} $h^{-1/2}$. Finally, the most noticeable modification in the release rate is observed in the sample with the highest phosphorus content, $Si_{95}P_5$. The silica release rate from this sample decreases to 0.24 mg g^{-1} $h^{-1/2}$, and consequently, the amount of SiO_2 leached to water dramatically diminishes. These results clearly evidence that the P_2O_5 presence in amounts higher than 1.25% mol in silica mesoporous matrices is an important approach to reducing the silica leaching to water.

The smaller rate of silicon dissolution from P-containing samples compared to pure silica material could be due to the higher connectivity degree of the network, in agreement with the NMR data. These results are in good concern with those reported by others authors, who evidenced that the addition of certain impurities such as iron or aluminum into the silica network or grafted on its surface reduces the rate of silica dissolution and diminishes the solubility of silica at equilibrium.[33,55]

To explain the reduced silica leaching effect observed in P-containing mesoporous silica (P_2O_5 > 1.25% mol), we need also to consider the process of silica dissolution in aqueous medium that lead to degradation of pure silica in water. It is well-known that silica dissolution is a catalytic process and that it is mainly accelerated in the neutral and alkaline pH region by OH^- ions.[56−58]In the intermediate pH region (pH 5−8), the concentration of hydroxyl ions in water is low. However, the quantity is enough to catalyze the polymerization of silicic acid and the dissolution of silica. It can be considered that at pH < 5, where the content of hydroxyl ions in water is relatively low, the cleavage of siloxane bonds in silica proceeds mainly through a substitution mechanism with the participation of water molecules. However, the lower silica dissolution observed in this acid pH region reflects the fact that water molecules are weaker nucleophilic agents in comparison with OH^- ions. The experiments here performed at pH close to 3.5, evidence that the phosphorus incorporation into the silica network above the lower limit (P_2O_5 > 1.25% mol) causes a modification on the chemical nature of the final oxide species, probably due to the slower electronegativity of P substituting atoms compared to Si ones. This could modify the mechanism of silica dissolution by increasing the silica acidity and therefore promoting the release of H_3O^+ cations to water instead of

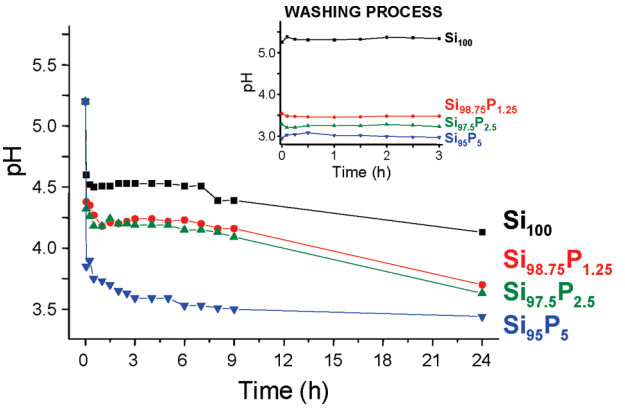

Figure 7. Variation of pH values in the water with the time after soaking of pure silica and P-containing silica mesoporous. (Inset) pH measurements during the washing process.

silicic acid, as in the case of pure silica matrices. In addition, as will be commented below, the results derived from the in vitro tests with cells carried out in buffered solution at pH 7.4 (DMEN medium) are in good agreement with the results here discussed. The increase in the acidity of silica by the presence of PO_4 units is also supported by pH and ζ−potential measurements. The evolution of pH after soaking the different Si_xP_y samples in water (initial pH 5.7) displayed in Figure 7 indicates that the pH decrease is more pronounced as the amount of P_2O_5 content in mesoporous matrices increases, which could be also confirming the effect of Si substitutions by P atoms into the SiO_2 network. This would be also supported by the ζ-potential measurements at different pH values (results not shown), which reveal that in the entire pH range, the net negative surface charge of P-containing mesoporous silicas is higher than that of pure silica Si_{100} sample. In fact, the isoelectric point (IEP) of samples shifts toward more acidic pH values when phosphorus is incorporated into the mesoporous matrix. Thus, the IEP values are 2.2 and ≤1 for Si_{100} and Si_xP_y ($y \geq 1.25$) samples, respectively. All these results point to the creation of new Brønsted acid centers that would notably decrease the silicic acid leaching in water and decrease the water degradability of these mixed matrices under "mild" conditions (water at 37 °C).

The structural, textural, and chemical stabilities of the Si_xP_y samples after 72 h of incubation in water at 37 °C were studied by XRD, TEM, N_2 adsorption, and NMR studies. XRD patterns of Si_xP_y (Figure 1b) show that meso-ordered arrangements are maintained after water treatment for all Si_xP_y materials. XRD patterns corresponding to the $Si_{95}P_5$ sample display a small peak centered at 1.4 °2θ, pointing to a slight loss of the 2D hexagonal meso-ordered arrangement compared with the initial material. However, TEM studies corresponding to this sample ($Si_{95}P_5$) after 72 h in water treatment confirm the presence of both mesophases (2D hexagonal and wormlike) as initially observed (Figure 8), although the percentage of 2D hexagonal structure is smaller than in the initial material. Figure 9 shows the N_2 adsorption isotherms corresponding to Si_xP_y samples ($y \leq 5$) after

(55) Higuchi, T. *J. Pharm. Sci.* **1963**, *52*, 1145–1147.
(56) Iler, R. K. *The Chemistry of Silica*; Wiley-Interscience: New York, 1979.
(57) Kim, J. M.; Ryoo, R. *Bull. Korean Chem. Soc.* **1996**, *17*, 66–69.
(58) Shen, S. C.; Kawi, S. *J. Phys. Chem. B* **1999**, *103*, 8870–8876.

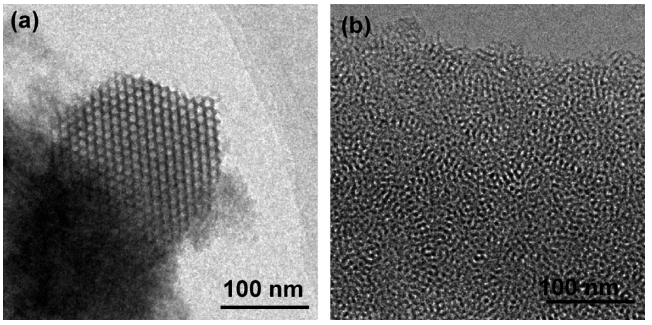

Figure 8. TEM images of $Si_{95}P_5$ material after 3 days in water treatment showing the presence of two mesophases: (a) 2D hexagonal structure and (b) wormlike structure.

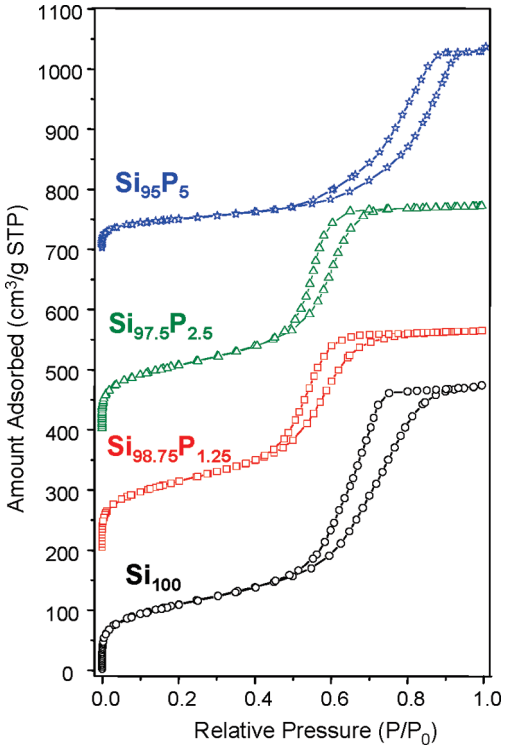

Figure 9. N_2 adsorption isotherms of Si_xP_y materials ($y \leq 5$) after being soaked in water for 72 h. The isotherms for samples $Si_{98.75}P_{1.25}$, $Si_{97.5}P_{2.5}$, and $Si_{95}P_5$ were vertically offset by 200, 400, and 700 cm^3/g STP, respectively.

being soaked in water during 72 h. All curves remain the shape of type IV isotherms with H1 type hysteresis loops observed before performing the stability studies the water. The textural data displayed in Table 2 reveal that S_{BET} and V_P values of Si_xP_y samples ($y \leq 2.5$) after soaking in water are similar to those of the original materials. On the contrary, $Si_{95}P_5$ sample undergoes a surface area reduction of around 90 m^2/g after water treatment, which could be related to the coexistence of wormlike and 2D hexagonal *p6mm* phases in this sample. TEM studies have demonstrated the preservation of both mesophases even after being submitted to water treatment (Figure 8).

Pure silica sample (Si_{100}) experiences a decrease in the pore diameter (D_P) from 6.70 to 6.34 nm and an increase in the wall thickness (t_{wall}) of ca. 1 nm after 72 h of soaking process, which is accompanied by a noticeable increase in

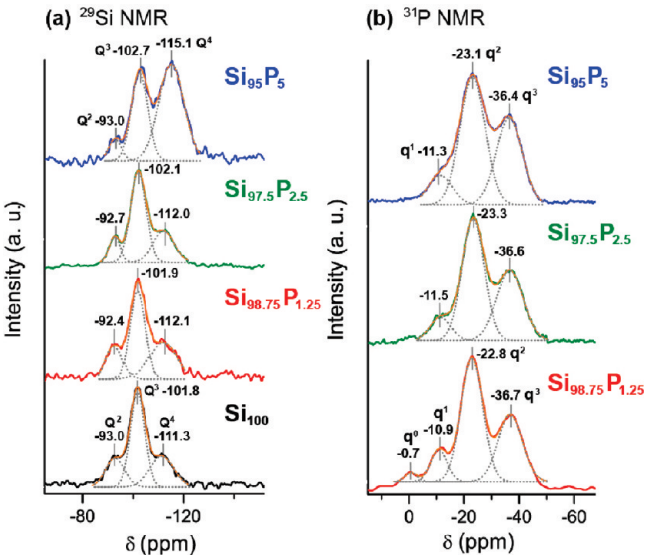

Figure 10. ^{29}Si MAS NMR (a) and ^{31}P MAS NMR spectra (b) of Si_xP_y samples after being soaked in water for 72 h.

the unit cell parameter (a_0). The pore diameter of the sample with the smallest phosphorus amount ($Si_{98.75}P_{1.25}$) decreases from 5.25 to 4.80 nm after being submitted to the water treatment. In this case, there are not significant variations in the a_0 values, whereas the t_{wall} experiences a slight increase with the soaking time. In the case of $Si_{97.5}P_{2.5}$ sample, the pore diameter of the main channels decreases from 5.50 to 5.20 nm after water treatment and there is also a decrease in the t_{wall} that is tightly related to the decrease in the a_0 values. In the case of $Si_{95}P_5$ sample, in which coexist both *p6mm* and wormlike phases, the treatment of data from N_2 adsorption analyses become more difficult. An increase in the main pore diameter attributed to the *p6mm* phase (D_P) together with a slight decrease in the t_{wall} is observed after the water treatment, which is accompanied by an increase in the a_0 values.

In general, the variations in the textural properties (D_P and t_{wall}) and a_0 due to the soaking process are more remarkable in pure silica sample (Si_{100}) than in samples that incorporate phosphorus and exhibit pure 3D bicontinuous cubic ($Si_{98.75}P_{1.25}$) or pure *p6mm* 2D hexagonal ($Si_{97.5}P_{2.5}$) symmetries. Certainly, the presence of PO_4 units could be contributing to some extent to the increase in the stability of the resulting structures. The loss of phosphorus during the initial step of water treatment could produce nonstructural phosphorus species not only as random structures, which would enhance the stability of the resulting pores, but also as phosphorus-rich surface species, which would be preventing the surface framework from hydrolysis. This fact would be in agreement with the significant decrease in the amount of silica leached to water observed in samples containing phosphorus compared to pure silica (Si_{100}) sample.

For further evaluating the effect of the water treatment in the chemical nature of the mesoporous frameworks,we recorded ^{29}Si and ^{31}P NMR spectra of Si_xP_y samples after being soaked in water during 72 h (Figure 10). As previously commented, the ^{29}Si NMR spectra of Si_xP_y

samples before soaking exhibited two main signals that can be ascribed to $Si(OSi)_3(OH)$ (Q^3) or $Si(OSi)(OP)(OH)_2$ and $Si(OSi)_4$ (Q^4) or $Si(OSi)_2(OP)(OH)$ species (Figure 5a). After 72 h of water treatment, all spectra display a new band at ca. −93 ppm that can be assigned to Q^2 [$Si(OSi)_2(OH)_2$] species (Figure 10a). Moreover, it can be noticed that there is an increase in the relative intensity of the signal corresponding to silicon in Q^3 or $Si(OSi)(OP)(OH)_2$ environments. This effect agrees with previously reported results in which water treatment caused the hydrolysis of ≡Si−O−Si≡ linkages into ≡Si−OH bonds with the consequent appearance of Q^2 species and the increase in the relative abundance of Q^3 or $Si(OSi)(OP)(OH)_2$ species.

Moreover, the decrease degradability rate in water at 37 °C of these P-containing samples could be related to the increase in the cross-linking degree of the silica network compared to pure-silica Si_{100} matrix, as confirmed ^{29}Si NMR spectroscopy. In order to support such affirmation, study under high humidity environment has been performed by indirect measurement of SiOH groups in the samples. The amount of water adsorbed in the sample has been determined by TG analyses (weight loss < 120 °C) and taken as a measure of amount of silanol groups in the samples. The results reveal that P-containing samples exhibit comparable behaviors, with the weight loss being ca. 30% up to 120 °C. However, this weight loss is two times higher (∼60%) in the case of pure-silica Si_{100} sample. The sequence of weight loss begins at ∼40 °C to ∼100 °C and is assigned to a removal of physically adsorbed water, followed probably by gradual removal of water molecules bound with the surface Si−OH and P−OH groups. These results indicate that Si_{100} sample present more points of water adsorption than P-containing samples as a consequence of the higher density of free silanol groups (Si−OH) of the former. In the case of $SiO_2-P_2O_5$ mesoporous samples, an increase in the cross-linking degree of the silica network due to the presence of P_2O_5 could be the responsible of the reduction of the water adsorption capacity. The mechanism involves that adsorbed water molecules can attack the ≡Si−O−Si≡ linkages, which are then converted to ≡Si−OH bonds, leading to the rehydroxilation of the surface and consequently to the hydrolysis of the surface framework.[59] The presence of PO_4 units forming covalent networks in $Si_{98.75}P_{1.25}$ and $Si_{97.5}P_{2.5}$ samples, as demonstrated by ^{31}P NMR spectroscopy, could reduce the attack of water molecules on the silica framework, contributing to the stabilization of the mesoporous structures.

Moreover, for the $Si_{95}P_5$ sample it can be observed a slight shift toward upfields from −114.1 to −115.1 ppm of the signal assigned to $Si(OSi)_{4-x}(OP)_x$, (with $x = 1-3$) units that could be ascribed to a higher incorporation of phosphorus into the silica network. This fact would agree with the decrease in the relative amount of phosphorus remaining in $Si_{95}P_5$ sample, determined by XRF in comparison to $Si_{98.75}P_{1.25}$ and $Si_{97.5}P_{2.5}$ matrices (Table 4). In this sense, the increase in the number of phosphorus centers in the $Si_{95}P_5$ material during the soaking process could be inducing the dehydrolization of Si−OH bonds to form ≡Si−O−Si≡ or ≡Si−O−P≡ linkages. In addition, the greater presence of PO_4 units into the mesoporous silica framework could be also resulting in an almost totally disordered structure, as confirmed by XRD.

These results reveal that the $SiO_2-P_2O_5$ mixed oxides exhibit slower degradability in aqueous media under "mild" conditions that pure silica mesoporous material. Besides, there are not significant changes in their corresponding mesostructures as confirmed by XRD, N_2 adsorption, and TEM probably because of the "mild" conditions (72 h in water at 37 °C). These assays provide novel insights into potential applications of these mesoporous materials in the biomedical field (drug delivery, bone-regeneration, tissue engineering, etc.).

In vitro Biocompatibility Assays. Si_xP_y materials present different reactivity in water depending on the P-content present in their composition. A reduced SiO_2 lixiviation has been observed when the phosphorus content is increased above 1.25% mol. When these materials are intended for biomedical applications an excessive local silica release could provoke a cytotoxic effect in the surroundings. With the aim of studying the effect of silica release in the cellular function of osteoblastic cells, biocompatibility assays have been performed by using different doses of each material in powder from 1.25 to 12.5 mg/mL. Preliminary biocompatibility assays have been achieved by studying the LDH enzymatic activity in the culture medium at short incubation times (2 days). The results derived from such tests are related to the membrane cellular rupture (cytotoxicity). Moreover, cell viability assays measuring cellular mitochondrial activity after 2 and 6 days were carried out.

LDH levels measured in the culture medium after 2 days are plotted in Figure 11a. The results indicate that cytolysis degree is lower for $Si_{95}P_5$ sample, independently of the material concentration used compared to pure silica (Si_{100}) and $Si_{97.5}P_{2.5}$ samples, which exhibit nonsignificant differences. These results are in agreement with the reduced SiO_2 leaching levels in culture medium observed for $Si_{95}P_5$ sample compared to Si_{100} material (Figure 11b). The silica released from Si_{100} and $Si_{97.5}P_{2.5}$ samples to the culture medium are not significantly different, which could explain the similar behavior observed in the LDH assays. Moreover, Figure 11a shows that independently of the chemical composition of samples, the LDH levels increase with the increase in the materials concentrations. This could be explained because the amount of silica leached is greater when the concentration increases (Figure 11b) and therefore the number of particles per cell is also increased, which could produce higher toxicity degree.

As above-mentioned, LDH is an intracellular enzyme that is only released to culture medium when cellular damage occurs. Therefore, the results here presented demonstrate that $Si_{95}P_5$ material induces the lowest cellular damage among all the tested matrices, probably because of its reduced SiO_2 release.

(59) Zhuravlev, L. T. *Colloids Surf., A* **1993**, *74*, 71–90.

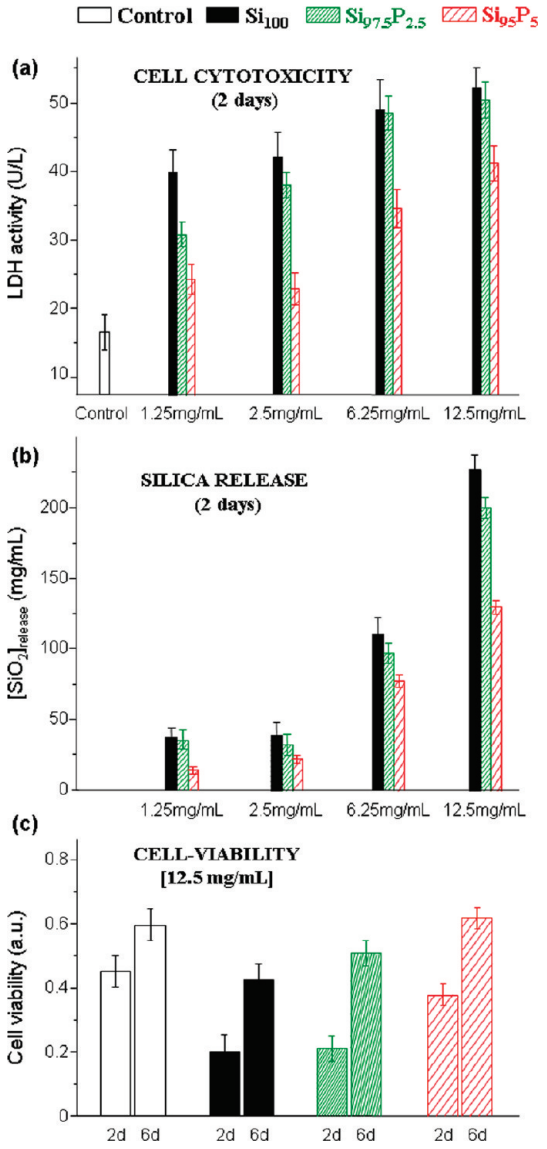

Figure 11. Biocompatibility assays by cell cultured of osteoblastic-like cells (HOS) seeded in presence of powder Si_xP_y materials at different concentrations. (a) Cytotoxicity tests by LDH activity determination on cultured medium after 2 days of incubation, (b) silica release in the culture medium after 2 days of incubation, and (c) cell-viability determined by mitochondrial activity of living cells after 2 and 6 days in incubation. All the results here represented are the mean values ± standard deviation derived from three independent experiments. The statistical differences between the mean values among groups were analyzed by ANOVA with SNK post hoc pair wise comparison test; statistical significance: only significant differences between groups are shown [$\rho < 0.05$].

Furthermore, cell viability assays have been performed at 2 and 6 days of incubation times for Si_{100}, $Si_{97.5}P_{2.5}$, and $Si_{95}P_5$ samples using the MTT method (Figure 11c). This method is based on mitochondrial redox activity of "living cells" which reduce the MTT to blue formazan. Figure 11c displays the measurements of cell viability after 2 and 6 days for the highest materials concentration (12.5 mg/mL), showing an evolution in the cellular proliferation with the incubation time for all tested samples. This behavior indicates that all these materials are biocompatible, with the $Si_{95}P_5$ sample exhibiting the highest cellular viability. This is in good agreement with the smallest cytolytic effect observed for this sample after 2 days (Figure 11a).

Conclusions

Nanostructured mesoporous silica networks with phosphorus substitutions have been synthesized by EISA method using nonionic triblock copolymer P123 as structure directing agent. For a constant molar ratio between the network former precursors (TEOS + H_3PO_4) and the surfactant, the structural and textural properties of the resulting matrices are governed by the P/Si molar ratio. These materials display structures that evolve from 3D cubic to 2D hexagonal and wormlike structures when the substitution degree of silica by phosphorus centers increases.

The degradability tests performed in water at 37 °C reveal that the amount of SiO_2 released is noticeably reduced from samples with P_2O_5 contents higher than 1.25 mol %.

These results could be explained by the increase in the cross-linking degree together with an increase in the acidity of silica network by Si substitutions by P atoms.

Preliminary in vitro biocompatibility assays in osteoblastic cell culture (by measurement of LDH activity and mitochondrial function by reduction of MTT reagent) evidence the lowest cellular damage induced by the sample with the highest P-content. Moreover, cell viability assays evidence the biocompatible behavior of these materials under the tested conditions, as the sample with the highest P-content exhibits the highest viability rate. These materials are promising candidates to be applied in diverse technological fields including biomaterials science.

Acknowledgment. This work was supported by the Spanish CICYT through Project MAT2008-00736 and by the Comunidad Autónoma de Madrid through Project S-0505/MAT/0324. We also thank Fernando Conde (CAI X-ray Diffraction), CAI XRF, Universidad Complutense de Madrid, and CAI Electron Microscopy Center for their valuable technical assistance.